PCCP

CoNiCuCrS alloy nanoparticles: Synthesis and atomically resolved T/STEM studies

Journal:	*Physical Chemistry Chemical Physics*
Manuscript ID	CP-ART-05-2024-002042.R2
Article Type:	Paper
Date Submitted by the Author:	06-Aug-2024
Complete List of Authors:	Rufino da Silva, Carlos; Northern Arizona University, Applied Physics and Materials Science Bahena, Daniel; Centro de Investigacion y de Estudios Avanzados del Instituto Politecnico Nacional, Laboratorio Avanzado de Nanoscopía Electrónica (LANE) Velazquez-Salazar, Jesus; Northern Arizona University, Applied Physics and Materials Science Karna, Dilip; Northern Arizona University, Applied Physics and Materials Science Agyei-Mensah, Joelin; Northern Arizona University, Applied Physics and Materials Science Yacaman, Miguel; Northern Arizona University, APMS

ARTICLE

CoNiCuCrS alloy nanoparticles: Synthesis and atomically resolved T/STEM studies

Received 00th January 20xx,
Accepted 00th January 20xx

DOI: 10.1039/x0xx00000x

Carlos E. Rufino da Silva [a], Daniel Bahena [b], J. Jesús Velázquez Salazar [a], Dilip Karna [a], Joelin Agyei-Mensah [a], and Miguel José Yacamán [a,*]

In this paper, we reported the synthesis and characterization of CoNiCuCrS nanoparticle alloys using scanning transmission electron microscopy (STEM) techniques. The nanoparticles form hexagonal platelets with an average size of 34.5 nm. Atomic resolution STEM imaging reveals an ordered FCC crystal structure with a lattice parameter of 0.93 nm, consistent with a $(CuCo)_6Ni_3Cr_1S_{13.333}$ intermetallic phase. The paper provided direct experimental evidence of the strain distribution at the atomic scale using advanced STEM techniques. The findings are consistent with previous studies, confirming the presence of small but significant strains in High Entropy Alloys (HEA). By studying nanoparticles, we achieved atomic-resolution imaging and characterization, which is challenging with bulk HEA samples. The work suggested defects like stacking faults and partial dislocations, stabilized by the presence of sulphur in our sample, play an important role in the mechanical properties of HEA. This research demonstrated that nanoparticles can be used as a model for studying bulk properties of HEA, providing insights into local strain effects, crystal growth dynamics.

Introduction

Multimetallic alloys (MMA) are becoming one of the most important topics in modern material science. Indeed, multimetallic alloys such as the Heusler alloys [1-3], the quasicrystals [4, 5], and the High Entropy Alloys (HEA) [6-12] are among the more studied systems. Many of these alloys have already reached the market. One of the important principles is that in multimetallic alloys, the lattices would be highly distorted because atomic sizes are all different from one another. Therefore, a local strain will reduce the dislocation mobility with the corresponding increase in strength. However, this local strain can have its origin due to several factors such as domain structure, and lattice mismatch between their atomic compounds as said before. A very interesting review on lattice strain in nanoparticles was presented by Nelli et al. [13]. Theoretical calculations have predicted the local distortions [11]. However, the exact nature of the lattice distortion is still not fully understood. Owen and Jones report that, at present, there is no convincing direct evidence within the literature that supports the hypothesis that the crystal structures of multicomponent HEAs are severely distorted. Experimental results seem to indicate small displacements, which are of a similar magnitude to those observed in conventional binary and ternary alloys [1,2]. Miracle et al. and George and co-workers reached the same conclusion [6, 14, 15]. On the other hand, it is well known that multimetallic alloys are less ductile, which suggests the existence of a mechanism that hinders dislocation mobility. A particularly important technique to solve this problem is transmission electron microscopy (TEM), which can provide local information at the atomic level. Preparing samples from bulk alloys for TEM examination can be challenging. Frequently, electropolishing is used, but the sample must be cut, dimpled, and sometimes polished, and some damage can be introduced. In addition, it is not common to produce large areas thin enough for atomic resolution microscopy. Another common method is to use a focused ion beam (FIB) to produce thin lamellas, but the Ga+ ion beam used for milling can produce radiation-induced defects that might alter the original state of the alloy. In addition, due to its brittleness, multimetallic alloys often break during the milling process, and it is not possible to obtain a large sample.

One possible way to advance the basic knowledge of MMA is to study nanoparticles of multimetallic alloys. These are thin enough to obtain atomic-resolution images and apply advanced characterization techniques. One might argue that in nanoparticles, the surface has a very important role, unlike in bulk alloys. However, large enough of ~100 nm can be prepared and will represent an intermediate situation.

In this paper, we report the preparation and characterization of CoNiCuCrS nanoparticles, a quinary alloy that presents a system in which four of the atomic radii are similar, and one (the sulphur) is larger. We employed a chemical technique to produce the alloy, and its characterization was carried out using Scanning Transmission Electron Microscopy (STEM) based techniques.

Materials and methods

Chemicals and materials:

Copper (II) chloride ($CuCl_2$), cobalt chloride ($CoCl_2$), nickel chloride ($NiCl_2$), chromium chloride ($CrCl_2$), Oleylamine (OLA), acetone and ethanol, were purchased from Sigma-Aldrich. All reagents were analytical grade.

Synthesis of CuCoNiCr NPs:

[a] Department of Applied Physics and Materials Science, Northern Arizona University, Flagstaff, AZ, 86011, USA.
[b] Laboratorio Avanzado de Nanoscopía Electrónica (LANE), Centro de Investigación y de Estudios Avanzados del Instituto Politécnico Nacional, Av. Instituto Politécnico Nacional, C. P. 07360, Ciudad de México, Mexico.
* Corresponding author. E-mail address: Miguel.Yacaman@nau.edu (M.J. Yacamán).

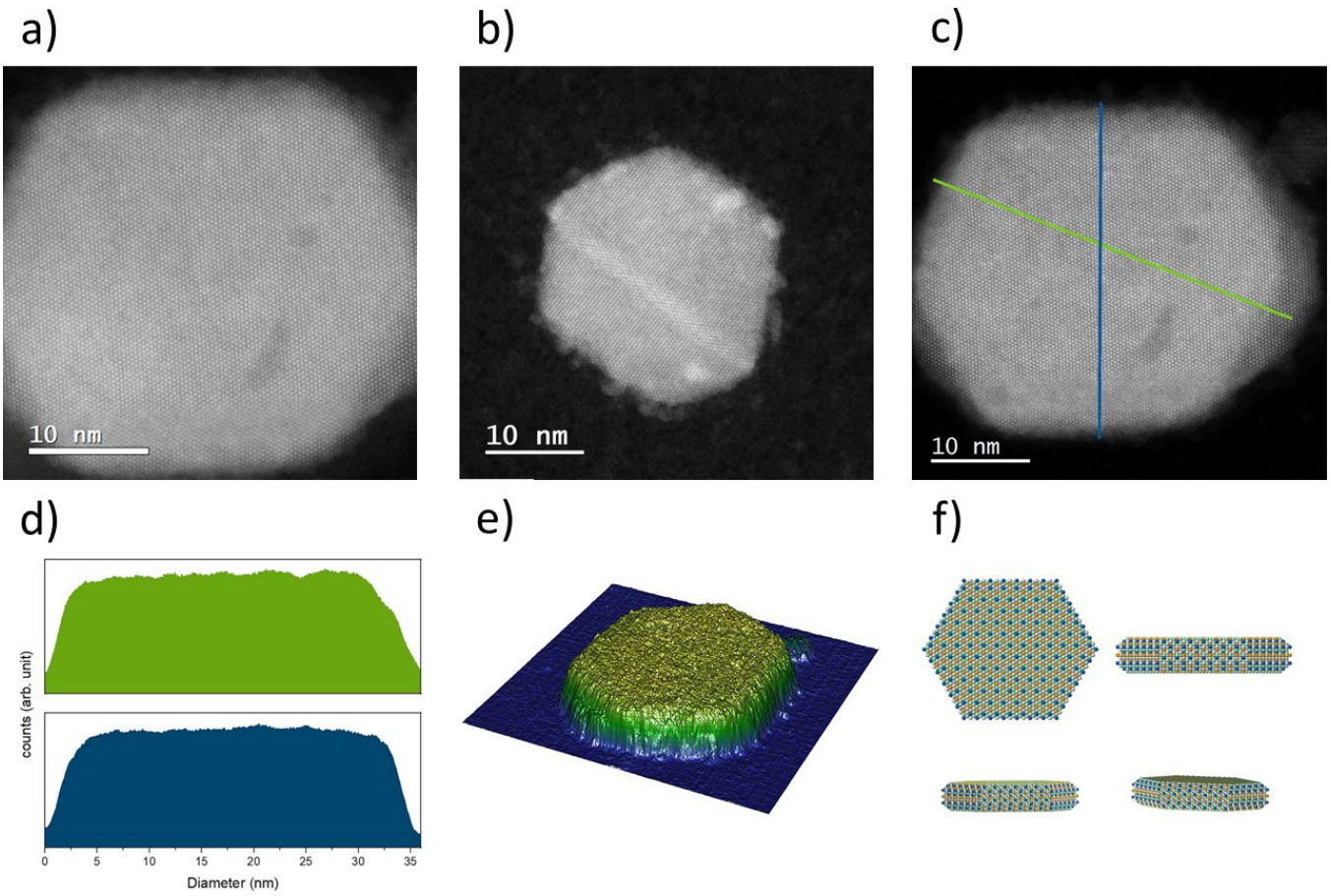

Figure 1: STEM/HAADF image of the CoNiCuCrS hexagonal nanoparticles alloys. The hexagonal shape of the structure is highlighted in (a), structure showing a twin boundary is shown in (b), lines of profile analyses are shown in (c), profile plot is shown in (d), 3-dimensional reconstruction of the STEM image in (e), and 3-dimensional modelling of the structure in (f).

In a 20 mL glass vial, 100 µL of $CuCl_2$ (100 mM in ethanol), 100 µL of $CoCl_2$ (100 mM in ethanol), 100 µL of $NiCl_2$ (100 mM in ethanol), 100 µL, and $CrCl_2$ (100 mM in ethanol) were added to 5 ml of OLA mixed at room temperature.

The solution was heated at 120 °C for 10 min. Then, the temperature is increased to 220 °C, after 7 min, 200 microliters of 1-dodecanethiol was added to the hot solution. Then, the mixture was heated for 30 min and cooled to room temperature. Finally, the solution was washed with acetone- ethanol three times by centrifugation and dispersed with chloroform.

Characterization:

Structural features of the produced NPs were characterized by Aberration-Corrected STEM imaging in High-Angle Annular Dark-Field (HAADF) mode was performed on a JEOLARM200F microscope, operating at 200 kV. The collection semi-angle for HAADF imaging was set to the 68−280 mrad range to avoiding the contribution of diffraction contrast.

Computational details:

The STEM simulated images were obtaining using ReciPro [16], a free and open-source multipurpose crystallographic software. The software was set to STEM mode, and the STEM image was chosen as elastic & TDS. The thickness of the theoretical sample was 41nm, and the angular resolution was set at 0.4 mrad.

Results

The produced nanoparticle alloys form hexagonal platelets, shown in Fig. 1a, 1b and 1c, with an average size of 34.5 nm. In some cases, the platelet shows a twin structure as seen in Fig. 1b. The STEM/HAADF images at low magnification, Fig. 1a, 1b and 1c, together with the structural profile plot, shown in Fig. 1d, confirm that the platelet is very flat. During the growth of nanoparticles twins are necessary. The twins in nanoparticles play a similar role to dislocations in bulk crystals [17]. The formation of flat hexagonal plates has been explained in terms of the formation of twin planes in the [111]-type faces [18]. Twins parallel to the surface are formed as shown in Fig. 2. Due to the sixfold symmetry of the FCC lattice, 3 twins are formed. At the terminations of those twins convex (A-type) and concave (B-type) terminations are formed. The growth along the facets will be much faster than in the perpendicular direction [19]. Due to their flat surfaces, sharp corners and smooth edges, these structures tended to be oriented in the <111> direction.

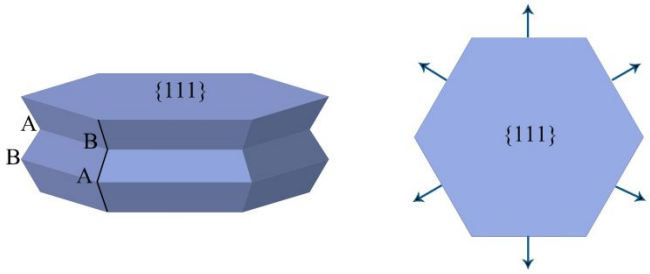

Figure 2: Model of hexagonal shape growth in an FCC symmetry showing both the side (left) and the top (right) view. The parallel twins causes alternating sides to have alternating A-type (concave), and B-type faces (convex).

A 3-dimensional reconstruction of the structure is shown in Fig. 1e, and a model of the structure shape is shown in Fig. 1f. The Energy dispersive spectroscopy (EDS) chemical analysis indicates that all five elements are present in the particle as shown in Fig. 3. When a line profile is obtained along a line crossing the nanoparticle, it is apparent that the distribution of elements is not constant along the alloy. However, despite the variations in the concentration, atomic resolution images show an ordered structure as shown in Fig. 4a. The Fast Fourier Transform (FFT), shown in Fig. 4b, of the image can be indexed as an FCC structure with a lattice parameter of 0.93 nm. The orientation is along a <111> orientation, and therefore, we can see hexagonal arrays of equally spaced atomic columns. We verify in 30 nanoparticles that the same crystal structure prevails. The lattice is consistent with the phase reported by Menzer [20]. We believe that in our case, the phase stoichiometry is $(CuCo)_6Ni_3Cr_1S_{13.333}$, which is consistent with the EDS analysis, shown in Fig. 3.

STEM/HAADF images are sensitive to both atomic number and the number of atoms on the column. To better understand the structure,

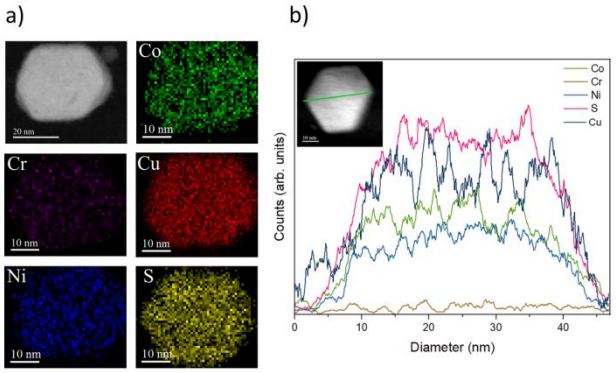

Figure 3: Energy dispersive spectroscopy elemental mapping for the CoNiCuCrS alloy (a). Elemental line scan along arbitrary section of the CoNiCuCrS alloy as shown in (b).

an intensity scan along the <110> direction, of Fig. 4a, is shown in Fig. 4c. There is an alternation of strong and weak spots. Since the particle is very flat, and thickness variations with that periodicity are extremely unlikely, we conclude that the variations are due to atomic number contrast. The HAADF signal intensity is $\sim I^2$, and since Cr, Ni, Cu, and Co are closely located on the periodic table, therefore we conclude that the weak spots correspond to columns that contain sulphur (plus some metals). The scan profile of the STEM image shows variations that confirm that atoms are not always distributed in the same way. This is more clearly shown in Fig. 4d, which shows hexagonal packings with different atoms. Nevertheless, the overall crystal structure is maintained. Fig. 4e shows the proposed unit cell oriented at the <111> direction, a simulation of the structure for the conditions of the STEM image, oriented at <111> direction, is shown in Fig. 4f. Also, the intensity scan along the <110> direction is shown in Fig. 4g. The theoretical image, as well as the intensity scan along the <110> direction, is in perfect agreement with the experimental image. To obtain more detailed information about the atomic column distribution, we obtain an atomically resolved image titling the sample slightly off the <111> axis. Around the <110> axis, Fig. 5a shows the image at this orientation, the hexagonal packing is still present, but the contrast between the atomic columns is less pronounced. In addition, the STEM-HHADF image shows that the lines of atoms are not perfectly aligned, and some disorder is present.

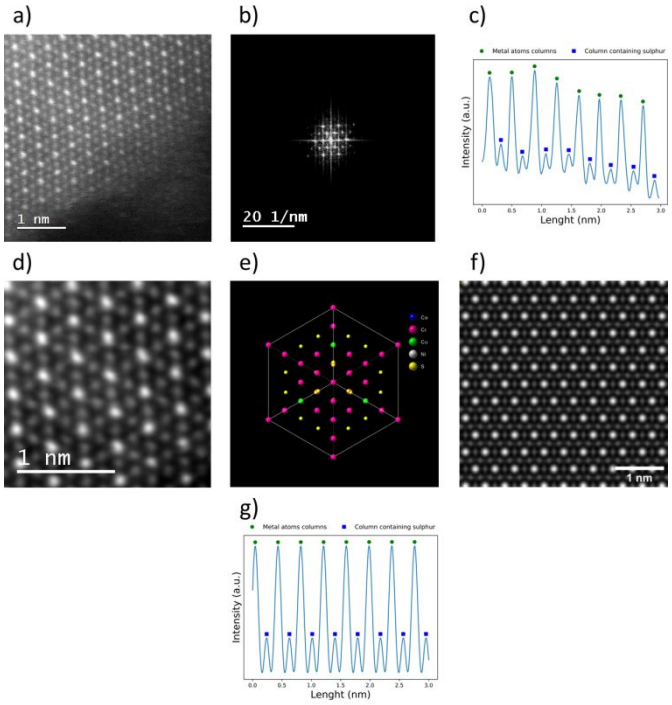

Figure 4: Atomic resolution image of CoNiCuCrS nanoparticle (a). FFT of Fig. 3a showing an FCC pattern with a 0.93 nm lattice parameter oriented at <111> direction (b). Structure intensity profile along <110> direction is shown in (c), the green squares represent the metal columns, and the blue squares the columns containing Sulphur. HR_STEM image showing hexagonal packings with different atoms (d). Theoretical model of the structure (e). HR-STEM image simulation along the <111> direction (f), and its profile intensity plot along <110> direction is shown in (g), the green squares represent the metal columns, and the blue squares the columns containing Sulphur.

The FFT in Fig. 5b shows that the zone axis is still <111> although other reflections have become stronger. A possible explanation is that the atoms in the atomic columns are slightly disordered. The misalignment will result in either diffuse scattering of extra reflections. To evaluate this hypothesis, we obtain a filtered image excluding all the main spots and including only scattering outside of those spots. The result is shown in Fig. 5c. The image has an apparent contrast in which some atoms along the <110> plane appear displaced. Since we are only including the (220) type spots, the contrast disappears if some atoms of the column are displaced. We believe that this is the result of the formation of stacking faults on the structure. STEM-HHADF images allow the determination of the strains on the sample.

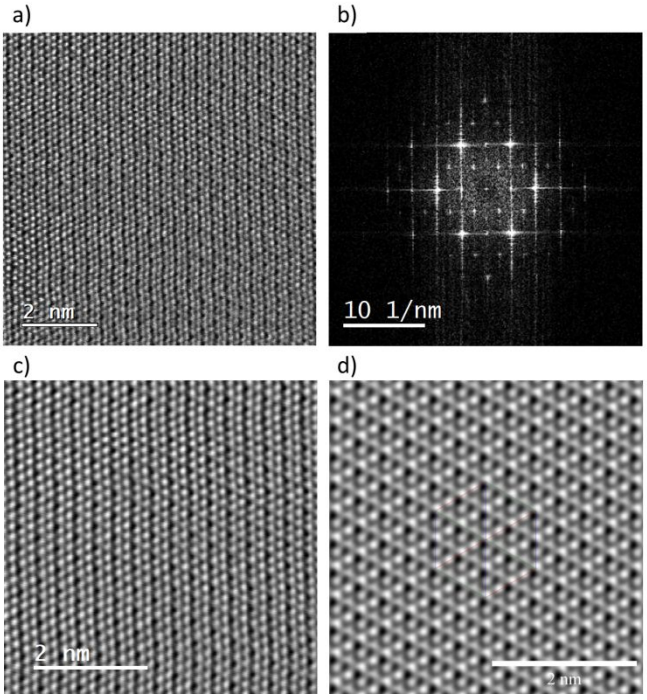

Figure 5: HR-STEM image of the CoNiCuCrS sample slightly tilted off the <111> axis (a). FFT of the HR-STEM image showing the zone axis still is <111> (b). Filtered image showing some atoms displaced along the <110> direction (c). Simulation of the tilted structure (d), the unit cell contours is seen in the centre of the figure.

To best understand the structure, we simulated the STEM image for Fig. 5a, as shown in Fig. 5d, and in agreement with the previous results, the crystal was found to be slightly tilted along the <111> axis according to the Euler angles: ϕ= 0,018 rad, θ= 0,951 rad, and ψ= 0,782 rad. The simulation reproduces the experimental image with reasonable agreement, even though the displacements were not considered in the simulation. A more quantitative understanding of the disorder in this material was obtained by applying a filter to the FFT diffraction pattern of Fig. 6a and calculating the inverse FFT only for its strongest Bragg diffraction peaks. The result is shown in Fig. 6b and shows the crystallographic plans along the <110> direction still are well ordered; however, they present smoothly perpendicular distortions indicating disorder in agreement with our last assumptions.

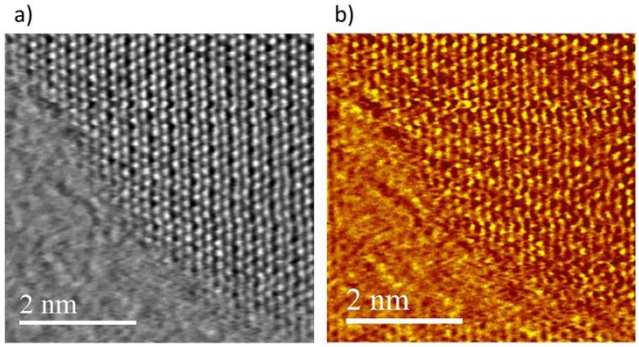

Figure 6: HR-STEM image of CoNiCuCrS nanoparticle (a), and filtering image showing the disorder on the structure.

We used the GPA method to plot the strain using several HHADF-STEM images [21, 22], as shown in Fig. 7. To avoid any fake effects, we use two images of the same nanoparticle rotated by 90º. Fig. 7a shows to the left a pseudo-coloured image of the strain along the nanoparticle shown in Fig. 1a, and Fig. 7b shows the quantitative plot along the line indicated on the image. The particle shows alternate

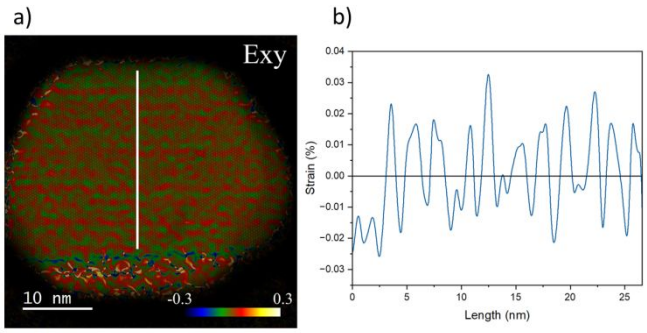

Figure 7: Calculated strain of CoNiCuCrS nanoparticle, shown in Fig. 1a, using GPA method (a). Percentual strain along the white line in the nanoparticle shown in Fig. 6a.

regions of compression and elongation. The magnitude is a maximum of ±2%. However, on average, the total strain will average out to approximately zero. On the other hand, the particle shows regions of very high compression near the surfaces, as shown in Fig. 5a, which might be related to the effects of surface energy.

Discussion

An intermetallic phase with the composition is $(CuCo)_6Ni_3Cr_1\ S_{13.333}$ with $Fd\bar{3}m$ crystal group, and a lattice constant of 9.47 was found in this work. A similar phase was reported back in the 1920s [20]. We have shown that the presence of sulphur stabilizes the formation of an intermetallic alloy rather than the classical idea of randomly distributed atoms. Sulphur resulted from the reduction agent used to fabricate the nanoparticles. In contrast with other cases in which the sulphur remains as a surface passivating agent [23-28], the sulphur integrates into the lattice structure. The atomic radius of S is 109pm, which is much lower than the other metals. The sulphur incorporation seems to be inconsistent with the Hume-Rothery rules [29, 30]. A particularly important fact is that despite a large variation in the local distributions of atomic species, the crystal lattice is preserved. In that sense, the phase is similar to the $L_0$1L1 family of phases. A significant difference is that the unit cell is preserved, but not the atoms forming it. This is probably because Co, Cu, and Ni has very close values of the atomic radius and will be easy to interchange atomic positions on the unit cell. We also found a distribution of strain along the particle. Cr has a larger atomic radius and, together with sulphur, might contribute to the local lattice strain. The values found in this work are consistent with the findings of Owen and Jones [12, 31] using Synchrotron methods and by other groups [32]. They are also consistent with theoretical calculations [11, 33].

It is well known that in nanoparticles, twins and stacking faults are necessary for maintaining crystal growth [34-37]. The stacking faults are a self-perpetuating step source. The STEM-HAADF images and the FFT streaks suggest the presence of stacking faults in the nanoparticles. We were able to measure atomic displacements, which are consistent with stacking faults and partial dislocations. Full dislocations are not present in nanoparticles. However, if present in bulk alloys, Sulphur and

twins (that are formed by sulphur displacement) can have the effect of slowing down dislocations. This aspect deserves more research on the defect structure of HEA.

Conclusions

We have synthesized multimetallic alloy nanoparticles and demonstrated their amenability to atomic-scale characterization, a feature unlikely achievable with bulk alloys. Therefore, they are a good model to study bulk HEA, providing us with valuable structural information such as local strain and stress. They show an overall crystalline structure, but the atoms are distributed in a variety of modes. They also have a highly defective structure, mainly due to the sulphur, which plays a role in mechanical properties. In addition, the possibility of additive manufacturing of HEA using powders and the usage as coatings [38] and thermal barriers [39] gives additional interest to the study of nanoparticles in this size range.

Author Contributions

Carlos E. Rufino da Silva: Writing – review & editing, simulations. Daniel Bahena: TEM measurements. J. Jesús Velázquez Salazar: Writing – review & editing, Synthesis. Dilip Karna: Writing – review & editing. Joelin Agyei-Mensah: Writing – review & editing, synthesis. Miguel José Yacamán: Writing – original draft, Writing – review & editing, investigation, formal analysis, coordination, supervision, conceptualization.

Conflicts of interest

The authors declare that they have no known competing financial interests or personal relationships that could have appeared to influence the work reported in this paper.

Acknowledgements

The authors acknowledge: The support of the Department of Energy (DOE), Office of Science Mission, Award No. DE-SC0023343, Mission DAC: Molecular Mechanisms of Moisture Driven DAC with Charged Polymers. The Army Research Office (ARO), PTE Federal Award No. W911NF-23-2-0014, Cognitive Distributed Sensing in Congested Radio Frequency Environments: FREEDOM. The National Science Foundation, Sponsor Grant No. 2025490, NNCI: Nanotechnology Collaborative Infrastructure Southwest (NCI-SQ). The Center for Materials Interfaces in Research & Applications (¡MIRA!) at Northern Arizona University (NAU) for allowing them to use its facilities.

Notes and references

1. Hirohata, A., et al., *Heusler alloy/semiconductor hybrid structures.* Current Opinion in Solid State & Materials Science, 2006. **10**(2): p. 93-107.
2. Bachagha, T. and Suñol, J.J., 2023. All-d-metal Heusler alloys: A review. *Metals*, **13**(1), p.111.
3. Tavares, S., K.S. Yang, and M.A. Meyers, *Heusler alloys: Past, properties, new alloys, and prospects.* Progress in Materials Science, 2023. **132**.
4. Tsai, A.P., *Icosahedral clusters, icosaheral order and stability of quasicrystals - a view of metallurgy.* Science and Technology of Advanced Materials, 2008. **9**(1): p. 20.
5. Steurer, W., *Quasicrystals: What do we know? What do we want to know? What can we know?* Acta Crystallographica a-Foundation and Advances, 2018. **74**: p. 1-11.
6. George, E.P., D. Raabe, and R.O. Ritchie, *High-entropy alloys.* Nature Reviews Materials, 2019. **4**(8): p. 515-534.
7. Brenne, F., A.S.K. Mohammed, and H. Sehitoglu, *High resolution atomic scale characterization of dislocations in high entropy alloys: Critical assessment of template matching and geometric phase analysis.* Ultramicroscopy, 2020. **219**.
8. Cantor, B., et al., *A Brief History of Alloys and the Birth of High-Entropy Alloys*. High-Entropy Alloys. 2014. 1-12.
9. Cantor, B., et al., *High-Entropy Alloy Solid Solutions*. High-Entropy Alloys. 2014. 91-118.
10. Yeh, J.W., et al., *Nanostructured high-entropy alloys with multiple principal elements: Novel alloy design concepts and outcomes.* Advanced Engineering Materials, 2004. **6**(5): p. 299-303.
11. Farkas, D. and A. Caro, *Model interatomic potentials and lattice strain in a high-entropy alloy.* Journal of Materials Research, 2018. **33**(19): p. 3218-3225.
12. Owen, L.R. and N.G. Jones, *Lattice distortions in high-entropy alloys.* Journal of Materials Research, 2018. **33**(19): p. 2954-2969.
13. Nelli, D., Roncaglia, C., & Minnai, C. (2023). Strain engineering in alloy nanoparticles. *Advances in Physics: X*, *8*(1), 2127330.
14. Miracle, D.B. and O.N. Senkov, *A critical review of high entropy alloys and related concepts.* Acta Materialia, 2017. **122**: p. 448-511.
15. George, E.P., W.A. Curtin, and C.C. Tasan, *High entropy alloys: A focused review of mechanical properties and deformation mechanisms.* Acta Materialia, 2020. **188**: p. 435-474.
16. Seto, Y. and Ohtsuka, M., 2022. ReciPro: free and open-source multipurpose crystallographic software integrating a crystal model database and viewer, diffraction and microscopy simulators, and diffraction data analysis tools. *Journal of Applied Crystallography*, *55*(2), pp.397-410.
17. vandeWaal, B.W., *Cross-twinning model of fcc crystal growth.* Journal of Crystal Growth, 1996. **158**(1-2): p. 153-165.
18. Lofton, C. and W. Sigmund, *Mechanisms controlling crystal habits of gold and silver colloids.* Advanced Functional Materials, 2005. **15**(7): p. 1197-1208.
19. Elechiguerra, J.L., J. Reyes-Gasga, and M.J. Yacaman, *The role of twinning in shape evolution of anisotropic noble metal nanostructures.* Journal of Materials Chemistry, 2006. **16**(40): p. 3906-3919.
20. *Crystal structure data from: Menzer, G. (1926) Ueber die Kristallstruktur von Linneit einschliesslich Polydymit und Sychnodymit.. 64:506 - 507.*
21. Hytch, M., et al., *Measuring lattice distortions from HR(S)TEM images.* Acta Crystallographica a-Foundation and Advances, 2011. **67**: p. C106-C106.
22. Chang, W.J. and T.D. Brown, *Reliability of the CFTM and GPA methods for strain analysis at ultra-thin layers.* Micron, 2011. **42**(5): p. 392-400

23. Lear, B., *Ligand control of the electronic structure near the Fermi energy in metallic nanoparticles.* Abstracts of Papers of the American Chemical Society, 2019. **258**.
24. Dreaden, E.C., et al., *The golden age: gold nanoparticles for biomedicine.* Chemical Society Reviews, 2012. **41**(7): p. 2740-2779.
25. Murphy, C.J., et al., *Gold nanorod crystal growth: From seed-mediated synthesis to nanoscale sculpting.* Current Opinion in Colloid & Interface Science, 2011. **16**(2): p. 128-134.
26. Guisbiers, G., et al., *Gold Copper Nano-Alloy, "Tumbaga", in the Era of Nano: Phase Diagram and Segregation.* Nano Letters, 2014. **14**(11): p. 6718-6726.
27. Edwards, P.P. and J.M. Thomas, *Gold in a metallic divided state - From Faraday to present-day nanoscience.* Angewandte Chemie-International Edition, 2007. **46**(29): p. 5480-5486.
28. Li, G. and R.C. Jin, *Atomically Precise Gold Nanoclusters as New Model Catalysts.* Accounts of Chemical Research, 2013. **46**(8): p. 1749-1758.
29. Mizutani, U. and U. Mizutani, *Hume-Rothery Rules for Structurally Complex Alloy Phases Introduction*. Hume-Rothery Rules for Structurally Complex Alloy Phases. 2011. 1-19.
30. Calvo-Dahlborg, M. and S.G.R. Brown, *Hume-Rothery for HEA classification and self-organizing map for phases and properties prediction.* Journal of Alloys and Compounds, 2017. **724**: p. 353-364.
31. Owen, L.R., et al., *An assessment of the lattice strain in the CrMnFeCoNi high-entropy alloy.* Acta Materialia, 2017. **122**: p. 11-18.
32. Tong, Y., et al., *Local lattice distortion in NiCoCr, FeCoNiCr and FeCoNiCrMn concentrated alloys investigated by synchrotron X-ray diffraction.* Materials & Design, 2018. **155**: p. 1-7.
33. Farkas, D., E. Bringa, and A. Caro, *Annealing twins in nanocrystalline fcc metals: A molecular dynamics simulation.* Physical Review B, 2007. **75**(18).
34. vandeWaal, B.W., *Cross-twinning model of fcc crystal growth.* Journal of Crystal Growth, 1996. **158**(1-2): p. 153-165.
35. Gibbs, J.W., et al., *The Three-Dimensional Morphology of Growing Dendrites.* Scientific Reports, 2015. **5**.
36. Lee, J.W., et al., *Growth process of the ridge-trough faces of a twinned crystal.* Acta Crystallographica a-Foundation and Advances, 2005. **61**: p. 405-410.
37. Ming, N., et al., *STACKING-FAULTS AS SELF-PERPETUATING STEP SOURCES.* Journal of Crystal Growth, 1988. **91**(1-2): p. 11-19.
38. Sharma, A., *High Entropy Alloy Coatings and Technology.* Coatings, 2021. **11**(4).
39. Shahbazi, H., et al., *High Entropy Alloy Bond Coats for Thermal Barrier Coatings: A Review.* Journal of Thermal Spray Technology, 2024. **33**(2-3): p. 430-446.

Data will be made available on request.